Optics Letters

Multi-band perfect plasmonic absorptions using rectangular graphene gratings

Sheng-Xuan Xia,[1] Xiang Zhai,[1] Yu Huang,[1] Jian-Qiang Liu,[2] Ling-Ling Wang,[1,*] and Shuang-Chun Wen[1]

[1]Key Laboratory for Micro-Nano Optoelectronic Devices of Ministry of Education, School of Physics and Electronics, Hunan University, Changsha 410082, China
[2]College of Science, Jiujiang University, Jiujiang 332005, China
*Corresponding author: llwang@hnu.edu.cn

Received 26 June 2017; revised 7 July 2017; accepted 7 July 2017; posted 7 July 2017 (Doc. ID 301023); published 1 August 2017

We propose to achieve multi-band perfect plasmonic absorptions with peak absorptivity >99% via the excitation of standing-wave graphene surface plasmon polaritons using single-layer graphene-based rectangular gratings. For the case with continuous gratings, perfect absorptions are only allowed for even-order modes, while the absorptions are quite low for odd-order modes because the fields are out-of-phase. However, for gratings with bottom-open configuration, four-band perfect absorptions containing both the even- and odd-order modes can be realized, which are found to be highly sensitive to the incident angle. The simulated results agree very well with the theoretical analyses by considering the phase path of the plasmonic waves. This multi-band absorber is a promising candidate for future plasmonic devices.

OCIS codes: (240.6680) Surface plasmons; (010.1030) Absorption; (230.1950) Diffraction gratings.

https://doi.org/10.1364/OL.42.003052

Excitation of electromagnetic waves known as surface plasmon polaritons (SPPs) being confined to and propagating along metallic surfaces is one of the ways that light strongly interacts with matters. SPPs exhibit a resonant behavior when the electric restoring force equals the Lorentz force caused by an incident field. However, the momenta of incoming free-space waves are usually much larger than those of SPPs. Several wave-matching mechanisms have been proposed to bridge this gap, such as the prism-coupling configuration, and the use of a dipole emitter or metallic nanostructures [1]. Besides, one of the common methods is the use of diffractive gratings, which can provide the in-plane momentum required for the incident radiation to excite SPPs [2].

However, the metal-based SPPs suffer a lot from their limited tunabilities and surface effect. Such shortcomings restrict the further development of plasmons, and it is necessary to find new plasmonic materials [3]. Owing to the one-atom thick nature, SPPs generated in highly doped graphene possess some attractive properties such as dynamical tunabilities, extreme confinements, and relatively low losses in mid-infrared and terahertz regions [4,5], which make them promising candidates for applications such as switches [6], light sources, and absorbers [3]. However, a monolayer graphene is poorly absorbing (about 2.3%) [7], which greatly weakens its vital role in thermal light emitters and photodetectors [3]. To transform it into a perfect absorber, different ways of achieving full absorptions have been suggested. Conventional methods include the patterning of graphene nanostructures such as ribbons [8] and disks [9], and the use of conductive gratings [10]. Besides, absorption enhancement is also obtained by stacking multilayer graphene sheets [8]. However, most of reported studies only focused on the single-band full absorption. Although several efforts have been made to achieve dual-band absorbers, the maximum absorptions are attributed respectively to the localized resonances in individual graphene configurations [11]. As far as we know, there is no report on three or more channel perfect absorbers using a single graphene sheet/island.

In this Letter, we propose that triple-band perfect plasmonic absorptions can be achieved using continuous rectangular graphene gratings. We will show that this absorber works effectively only for the even-order modes. We further prove that four-band perfect absorptions can be achieved in both the even- and odd-order modes by introducing an opening in the bottom of the grating. Considering the phase path of the plasmonic waves, the simulated results are well explained and the agreement with the theoretic analyses is nearly perfect.

Figure 1 illustrates the schematic view of the perfect absorbers. A monolayer graphene is attached to one-dimensional dielectric gratings with permittivity ε_2, under which a metallic substrate (Au) is used to reflect the transmitted light. The related geometric parameters are the grating period Λ, the grating width W, the grating height H, and the dielectric thickness D. In our simulations, we set $\Lambda = 0.2\ \mu$m, $W = 0.1\ \mu$m, $H = 0.5\ \mu$m, $D = 1.75\ \mu$m, $\varepsilon_1 = 1$, and $\varepsilon_2 = 2.25$ and keep them unchanged unless otherwise specified. All the corners are rounded with a 10 nm radius; thus, our analyses have reasonably neglected any effects that may arise due to the possible lattice discreteness and distortion in a real curved graphene [12]. Experimentally, this structure can be reached with present day technology, as reflection gratings with similar parameters

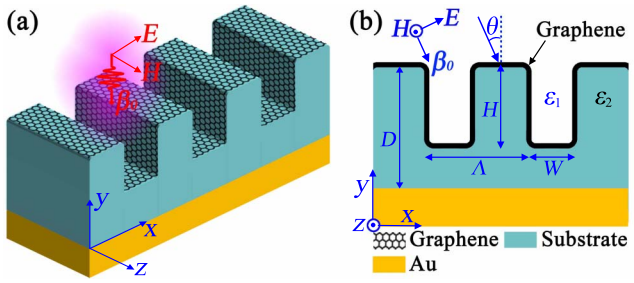

Fig. 1. (a) Side view and (b) front view of the absorber.

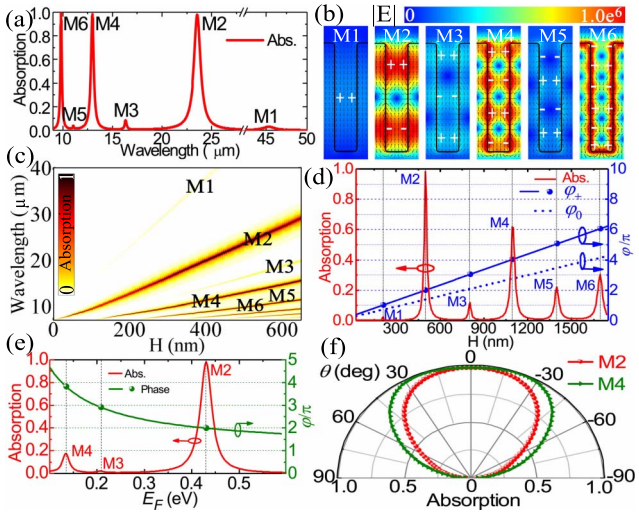

Fig. 2. (a) Normal-incidence absorption of the proposed system. (b) $|E|$ field for the first six modes at the maximum absorption, respectively. The + and − symbols sketch the resonant phase of E_x, while the arrows show the power follow. (c) Absorption map of the grating versus both the wavelength and H. Absorption (left) and phase path (right) as a function of (d) H and (e) E_F, respectively. (f) Absorption of the first two even-order modes as a function of θ.

have already been prepared by using electron beam lithography [13]. In addition, with the configurations of graphene onto complex three-dimensional pillars, large-area graphene sheet wrapped on rectangular gratings can be directly grown by the CVD method [14]. To ensure the excitation of graphene surface plasmon polaritons (GSPPs), the structure depicted in Fig. 1 is assumed to be illuminated by a transverse magnetic-polarized wave with wave number β_0 and an incident angle θ with respect to the y-direction.

Besides, the graphene film is modeled within the random-phase approximation by optical conductivity σ_g [4,15], which depends on the Fermi energy E_F and carrier lifetime τ *et al.* (which are respectively fixed as 0.43 eV and 0.645 ps unless otherwise specified). All the other graphene parameters and the COMSOL software settings are set the same as those in our previous work [15]. Note that in this Letter, we focus exclusively on the optical properties of the geometrical potential, thus assuming that graphene is homogeneously doped and has uniform distribution of the Fermi energy over its surface. The effect of a small change in E_F on trapped modes is the same as that for conventional plasmons on a flat graphene layer.

According to the Maxwell equations, the propagation constant of p-polarized SPPs supported by a single-layer graphene is $\beta_{\mathrm{SPP}} = \beta_0[\varepsilon_{\mathrm{avg}} - (2\varepsilon_{\mathrm{avg}}/\eta_0\sigma_g)^2]^{1/2}$, where $\varepsilon_{\mathrm{avg}}$ is the average permittivity in two sides of the graphene, and η_0 is the vacuum impedance [4]. Besides, the dispersion relation of SPPs is written as $k_h[\pm\exp(-k_h d) - 1] = 2i\varepsilon_{\mathrm{avg}}\beta_{\mathrm{SPP}}/\eta_0\sigma_g$, with $k_h = (\beta_{\mathrm{SPP}}^2 - \varepsilon_{\mathrm{avg}}\beta_{\mathrm{SPP}}^2)^{1/2}$ [6]. There are two solutions for this equation which correspond to symmetric and antisymmetric modes. These two modes exist when the couplings between the graphene sheets play a non-negligible role. After taking the coupling effects into account, the effective wave vectors of these two modes can be revised by small quantities with respect to β_{SPP} as a function of the space between the graphene sheets [6]:

$$\beta_{\pm} = \beta_{\mathrm{SPP}} + \frac{2i\varepsilon_{\mathrm{avg}}\beta_0/(\eta_0\sigma_g) - k_p(1 \mp u_p)}{(1 \mp u_p)\beta_{\mathrm{SPP}}/k_p \pm u_p\beta_{\mathrm{SPP}}d_\varepsilon}, \quad (1)$$

where the + and − symbols denote the symmetric and antisymmetric modes, respectively, d_ε presents the coupling distance between the grating walls in the dielectric with ε_1 or ε_2, and $k_p^2 = \beta_{\mathrm{SPP}} - \varepsilon_{\mathrm{avg}}\beta_0^2$, $u_p = \exp(-k_p d_\varepsilon)$.

To see how the plasmonic waves response to the incident light, simulations of the setup shown in Fig. 1 are carried out. Figure 2(a) shows the absorption spectrum of the first six order modes. It is very interesting to find that the absorptivity of the even-order modes are larger than 99%, while the odd-order modes are less than 8%, signaling that the absorptions of even-order modes are much higher than that of odd-order modes. However, it should be stressed that this selective absorption is quite different from the general situations with multi-plasmon resonances, where the most prominent absorption corresponds to the basic plasmon mode, while the higher-order absorptions become increasingly weaker [3]. All the peaks visible in Fig. 2(a) originate from the excitation of the main plasmonic resonance supported by the graphene rectangular gratings, since the gratings enable the diffraction and coupling of a plane wave into different order modes [2,13], resulting in strong optical absorptions.

To understand the absorption spectrum observed, spatial distributions of $|E|$ are plotted in Fig. 2(b) for the six absorption peaks, respectively. It is clearly shown that the absorptions reach their maxima once the standing wave graphene surface plasmon polariton (SWGSPP) modes are formed. When the incident radiation matches the frequency of a standing wave (SW), it resonantly excites the GSPP mode on the top and bottom surfaces and, thus, builds up strong plasmonic SWs in the gratings and further results in maximum absorption. Meanwhile, the field distributions along the grating sidewall show an SW pattern with clear nodes and antinodes for the even-order modes. Due to the asymmetric field distributions of the odd-order modes, the positions of notes and antinodes are not clear, especially for the higher-order modes. However, we find that the field in the two sidewalls distributes symmetrically about their centric lines, very similar to the symmetric modes supported in layered graphene sheets [6]. This special property of the SWs is much different from those formed in metallic gratings, where the resonances are significant not only in the trench surfaces but inside the gratings [13].

Since the plasmonic SWs are built up along the grating walls, the grating depth H plays a key role in producing these

localized waves. Figure 2(c) depicts the absorption map of the system as a function of both the incident wavelength and H. It is clear that the absorption peaks strongly depend on H. For shallow depth, for example, $H < 0.1$ μm, two peaks appear, but only the M2 mode is remarkable. As H increases, a set of absorption peaks occur due to the excitation of higher-order modes, and all modes shift to longer wavelengths, while their linewidths are broadened. Interestingly, we find that no matter whether H is small or big (even without the metallic substrate), the absorption of all even-order modes is much higher than that of odd-order modes. This selective absorption can be understood from the mechanism that forms the SWGSPPs. When the GSPP waves are generated on the top and bottom surfaces of the gratings, they propagate down and up and, in turn, resonantly build up plasmonic SWs. For the even (odd)-order modes, SWs are formed only when the optical path is even (odd) times the half-wavelength; in this condition, the generated plasmonic waves on the top and bottom surfaces are in-phase (out-of-phase), resulting in the strong (weak) absorption of the system.

As we know, the resonant wavelength λ of SW is determined by the maximum physical round-trip propagation distance that one could assume for a GSPP wave to propagate back and forth and, thus, is twice the value of H. Therefore, by denoting the phase path φ_ξ per sidewall along the depth of the grating as

$$\varphi_\xi = 2\pi \cdot \mathrm{real}(\bar{n}_{\mathrm{eff},\xi}) \cdot H/\lambda, \tag{2}$$

the maximum absorption can be estimated when $\varphi_\xi/\pi = M$ is satisfied, where $\bar{n}_{\mathrm{eff},\xi} = [n_{\mathrm{eff},\xi}(d_{\varepsilon 1}) + n_{\mathrm{eff},\xi}(d_{\varepsilon 2})]/2$ is the average effective refractive index; $n_{\mathrm{eff},\xi} = \beta_\xi(d_\xi)/\beta_0$ is the effective refractive index in the dielectric with ε_1 or ε_2; the subscript ξ denotes +, –, and 0 which, respectively, signify the GSPPs with symmetric modes, antisymmetric modes, and modes in single-layer situations; M stands for the mode order. To check this feature, the simulation results shown in Fig. 2(d) demonstrate clearly the absorptions with fixed $\lambda = 23.57$ μm, but different H. Meanwhile, we also plot the corresponding phase delay in the right label. This figure clearly displays that as H goes deeper, the SWs orderly form the six modes only when φ_ξ is an integer times of π. For modes M1-M6, the calculated φ_+ are 1.01π, 2.02π, 3.04π, 4.04π, 5.06π, and 6.06π, respectively, proving that the simulated results are in good agreement with theoretical data. Note that there still exist few errors due to the impact of the corners at the top and bottom gratings. If we neglect the symmetric coupling and only considering a single-layer graphene, the calculated φ_0 for M1-M6 modes are 0.72π, 1.39π, 2.09π, 2.76π, 3.47π, and 4.15π, respectively, which are smaller than the expected ones. Besides, the linear dependence of the wavelengths at the absorption maxima on H for all orders of the modes can be well explained by Eq. (2), as shown in Fig. 2(c).

Besides geometrical parameters, the most intriguing property of graphene-based plasmonic devices is their dynamic tunability. By employing an electrolytic gate, E_F as high as 0.8 eV was reached [5]. Thus, we conservatively assume E_F can be tuned from 0.1 to 0.6 eV. The simulated absorption line shown in Fig. 2(e) confirms the broad tuning range with fixed $\lambda = 23.57$ μm, but varying E_F. With decreasing E_F, the resonant mode can be tuned from M2 to M4. The appealing tunability is also strengthened by the corresponding phase paths, as shown in the right label of Fig. 2(e), where the maximum absorptions are shown to get their phases of 2.01π, 2.93π, and 3.83π. Note that in Figs. 2(d) and 2(e), the maximum absorption is not always achieved; one can just optimize D to reach perfect absorption. For example, for $H = 1.095$ μm ($E_F = 0.3$ eV), perfect absorptions for all even-order modes can be obtained when D is 5.22 or 21.225 μm (14.56 μm). Besides, we also explore the results for the feasibility of carrier lifetime. Perfect absorptions with peak absorptivity >99% (>90%) can be maintained when τ lies between 0.559 and 0.665 ps (within 0.328 and 1.013 ps).

Although being sensitive to the doping level, the absorptions hold a wild angle tolerance to the incidence. In Fig. 2(f), we show the angular dependence of absorbance for the first two even-order modes. For the low absorptions of the odd-order modes and the comparison below, other modes are not shown. With increasing θ, the absorptions of the two modes decrease monotonously. Note that the absorptions are high over a wide angular range; the absorbance of the M2 (M4) mode remains >90% when θ lies between ±30° (±42°). This wild angle tolerance allows different beam directions to be absorbed and, thus, could greatly facilitate the practical applications.

In the previous part, we have demonstrated that multichannel plasmonic absorptions can be achieved by using rectangular gratings composed of only a single, but continuous, graphene sheet. However, the perfect absorptions are only selectively achieved on the even-order modes. The low absorptions of the odd-order modes are because the plasmonic waves that directly form the SWs are out-of-phase. To overcome this deficiency, we have designed an absorber that can achieve perfect absorptions on both the even- and odd-order modes. As shown in Fig. 3(a), by etching off the bottom part of the grating

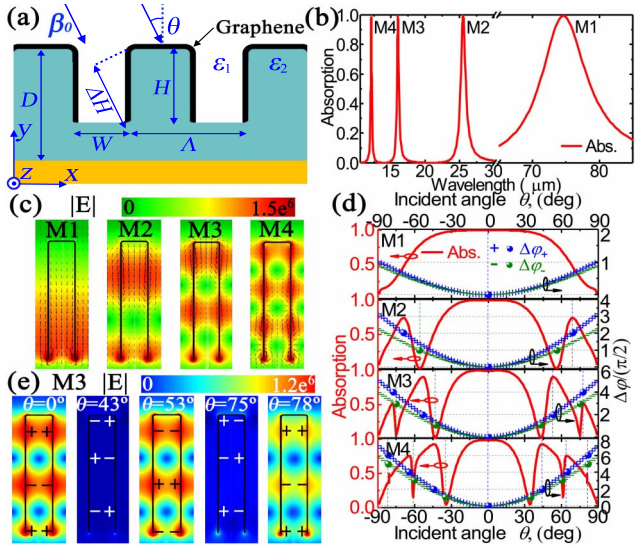

Fig. 3. (a) Front view of the absorber with bottom-open gratings. (b) Simulated normal-incidence absorption with optimized parameters as mentioned before, except $E_F = 0.53$ eV and $D = 14,000$ nm. (c) Electric field norms for the first four modes at the maximum absorption. The arrows show the power follow of the fields. (d) Absorption (left) and phase shift (right) for the first four modes as a function of θ. (e) Electric field distributions for the M3 mode at the maximum and minimum absorptions for different θ, respectively. The + and – symbols sketch the resonant phase of the electric field. Note that the scalar bars are kept the same in (c) and (e).

and, thus, introducing an open space at the trench bottom, GSPP waves can only be excited at the tops of the gratings. These plasmonic waves will propagate downward and be reflected by the cut end, producing the incoming and returning waves and further forming the SWs.

To illustrate this concept, we plot the simulated plasmonic response of the bottom-open gratings at $\theta = 0°$ in Fig. 3(b). Interestingly, four peaks with absorptivity >99% are observed. Different from the selective absorptions in the closed gratings, this bottom-open absorber allows both the even- and odd-order modes to achieve near-total absorption. To understand the physical mechanisms behind, electronic field distributions of the four absorption peaks are depicted in Fig. 3(c). As shown, the field along the surface of the grating shows SW patterns with clear nodes and antinodes, displaying one to four antinodes and nodes for modes from M1 to M4, respectively. Meanwhile, the fields distribute symmetrically along the two sides of the gratings and get stronger near the graphene edges.

The perfect absorptions of all these modes hence can be explained by considering the pivotal role of the open end. When the GSPP waves propagate downward and are reflected by grating terminals, a phase jump occurs. Thus, the single-trip phase path φ'_ξ per sidewall can be denoted as

$$\varphi'_\xi = [2\pi \cdot \mathrm{real}(\tilde{n}_{\mathrm{eff},\xi}) \cdot 2H/\lambda + \delta]/2, \quad (3)$$

and the maximum absorptions can be achieved only when $\varphi'_\xi/\pi = M$ is met, where $\delta = 0$ is the phase pickup at edge reflection [16]. The analytical phase paths φ'_+ obtained from Eq. (3) for the four modes at the wavelengths 74.64, 25.52, 16.01, and 12.11 μm are 1.01π, 2.01π, 3.06π, and 4.05π, respectively, showing a nearly perfect agreement.

Besides the choiceless absorptions at all order modes, this bottom-open graphene gratings are also highly sensitive to the incident angle. Figure 3(d) illustrates the absorption dependences on θ for the first four modes. Unlike the closed gratings, where the absorptions decrease monotonically with increasing θ [see Fig. 2(f)], the absorptions experience peaks and valleys with increasing θ. For the M-th mode, there are M absorption maxima and minima. To understand this, we define a phase shift $\Delta\varphi$ as the difference between the phase paths of the normal and oblique incidences:

$$\Delta\varphi = 2\pi \cdot \mathrm{real}(\tilde{n}_{\mathrm{eff},\xi}) \cdot H(1 - \cos\theta)/\lambda. \quad (4)$$

To clearly clarify the mechanism, we take M3 mode as an example and show the electric field distributions corresponding to the absorption maxima ($\theta = 0°$, 53°, 78°) and minima ($\theta = 43°$, 75°) in Fig. 3(e). Clearly, the SW resonances at the absorption peaks are much stronger than those of the absorption dips. For the absorption minimum at $\theta = 43°$ (75°), the calculated phase shift is $\Delta\varphi_- = \pi/2$ ($3\pi/2$), meaning that the resonant phase of the field has shifted $\pi/2$ ($3\pi/2$) relative to the situation with $\theta = 0°$ [along the counterclockwise direction of a semi-graphene ring, as the symbols + and − depict in Fig. 3(e)]. This phase shift results in the antisymmetric field distribution and further directly leads to the out-of-phase coupling between the two grating walls and, thus, the minimum absorption, while for the maximum absorption at $\theta = 53°$ (78°), the calculated phase shift is $\Delta\varphi_+ = \pi$ (2π), meaning that the resonant phase has shifted π (2π) relative to the normal incidence. This phase shift results in the symmetric field distribution, and leads to the in-phase coupling between the two grating walls, and further causes the maximum absorption. It is important to note that the phase shifts mentioned above are calculated by using Eq. (4) with antisymmetric (symmetric) models, since the minimum (maximum) absorptions are achieved only when the couplings between the two gratings walls are out-of-phase (in-phase). The phase shifts corresponding to all of the maximum and minimum absorptions of the four modes with respect to θ are shown in the right label of Fig. 3(d). Clearly, for all orders of the modes, the minimum (maximum) absorption occurs only when $\Delta\varphi_-$ ($\Delta\varphi_+$) is odd (even) multiples of $\pi/2$ and, thus, the couplings between the two gratings walls are out-of-phase (in-phase).

In conclusion, by using single-layer graphene-based gratings, multi-band perfect plasmonic absorptions with absorptivity >99% can be achieved when the SWGSPPs are formed. For the situation with closed grating configuration, perfect absorptions are only allowed for the even-order modes while, for gratings with bottom-open configurations and four-band perfect absorptions are realized for both the even- and odd-order modes. The proposed multi-plasmon absorber is a promising candidate for future use of photodetectors and thermal light-emitting sources.

Funding. National Natural Science Foundation of China (NSFC) (11074069, 11574079, 11664020, 61176116, 61505052).

REFERENCES

1. A. V. Zayats, I. I. Smolyaninov, and A. A. Maradudin, Phys. Rep. **408**, 131 (2005).
2. W. C. Tan, T. W. Preist, and R. J. Sambles, Phys. Rev. B **62**, 11134 (2000).
3. X. Luo, T. Qiu, W. Lu, and Z. Ni, Mater. Sci. Eng. R **74**, 351 (2013).
4. F. H. L. Koppens, D. E. Chang, and F. J. G. de Abajo, Nano Lett. **11**, 3370 (2011).
5. Z. Fang, S. Thongrattanasiri, A. Schlather, Z. Liu, L. Ma, Y. Wang, P. M. Ajayan, P. Nordlander, N. J. Halas, and F. J. García de Abajo, ACS Nano **7**, 2388 (2013).
6. B. Wang, X. Zhang, X. Yuan, and J. Teng, Appl. Phys. Lett. **100**, 131111 (2012).
7. K. F. Mak, M. Y. Sfeir, Y. Wu, C. H. Lui, J. A. Misewich, and T. F. Heinz, Phys. Rev. Lett. **101**, 196405 (2008).
8. H. Li, L. Wang, and X. Zhai, Sci. Rep. **6**, 36651 (2016).
9. S. Thongrattanasiri, F. H. L. Koppens, and F. J. G. de Abajo, Phys. Rev. Lett. **108**, 047401 (2012).
10. T. R. Zhan, F. Y. Zhao, X. H. Hu, X. H. Liu, and J. Zi, Phys. Rev. B **86**, 165416 (2012).
11. G. Yao, F. Ling, J. Yue, C. Luo, J. Ji, and J. Yao, Opt. Express **24**, 1518 (2016).
12. F. J. García de Abajo, ACS Photon. **1**, 135 (2014).
13. T. López-Rios, D. Mendoza, F. J. Garcia-Vidal, J. Sánchez-Dehesa, and B. Pannetier, Phys. Rev. Lett. **81**, 665 (1998).
14. J. Song, L. Zhang, Y. Xue, Q. Y. S. Wu, F. Xia, C. Zhang, Y.-L. Zhong, Y. Zhang, J. Teng, M. Premaratne, C. W. Qiu, and Q. Bao, ACS Photon. **3**, 1986 (2016).
15. S. X. Xia, X. Zhai, L. L. Wang, B. Sun, J. Q. Liu, and S. C. Wen, Opt. Express **24**, 17886 (2016).
16. J. Chen, M. Badioli, P. Alonso-Gonzalez, S. Thongrattanasiri, F. Huth, J. Osmond, M. Spasenovic, A. Centeno, A. Pesquera, P. Godignon, A. Z. Elorza, N. Camara, F. J. Garcia de Abajo, R. Hillenbrand, and F. H. L. Koppens, Nature **487**, 77 (2012).